ChemComm

Accepted Manuscript

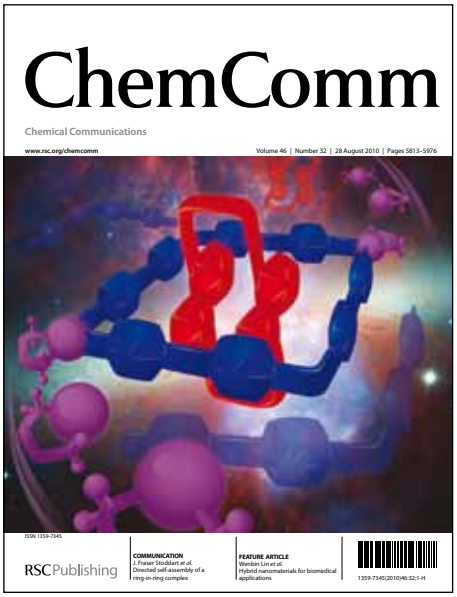

This is an *Accepted Manuscript*, which has been through the RSC Publishing peer review process and has been accepted for publication.

Accepted Manuscripts are published online shortly after acceptance, which is prior to technical editing, formatting and proof reading. This free service from RSC Publishing allows authors to make their results available to the community, in citable form, before publication of the edited article. This *Accepted Manuscript* will be replaced by the edited and formatted *Advance Article* as soon as this is available.

To cite this manuscript please use its permanent Digital Object Identifier (DOI®), which is identical for all formats of publication.

More information about *Accepted Manuscripts* can be found in the **Information for Authors**.

Please note that technical editing may introduce minor changes to the text and/or graphics contained in the manuscript submitted by the author(s) which may alter content, and that the standard **Terms & Conditions** and the **ethical guidelines** that apply to the journal are still applicable. In no event shall the RSC be held responsible for any errors or omissions in these *Accepted Manuscript* manuscripts or any consequences arising from the use of any information contained in them.

Journal Name

RSCPublishing

COMMUNICATION

Ionic Liquid Derived Carbons as Highly Efficient Oxygen Reduction Catalysts: First Elucidation of Pore Size Distribution Dependent Kinetics

Cite this: DOI: 10.1039/x0xx00000x

Received 00th January 2012,
Accepted 00th January 2012

DOI: 10.1039/x0xx00000x

www.rsc.org/

Zhiyong Zhang[a], Gabriel M. Veith[b], Gilbert M. Brown[a], Pasquale F. Fulvio[a], Patrick C. Hillesheim[a], Sheng Dai[a], and Steven H. Overbury[a*]

Metal-free N-doped carbons with controllable pore texture were derived from carbonization of ionic liquid and served as catalysts for oxygen reduction reaction (ORR) with an activity comparable to that of Pt/C. The investigation shows that both the ORR activity and kinetics are strongly correlated with the pore size distribution.

Nitrogen-doped carbons have recently been recognized as promising oxygen reduction catalysts for the replacement of costly Pt-based catalysts in alkaline environment.[1-6] To improve the performance of these carbon-based catalysts, research efforts have been focused on investigating active nitrogen–carbon bonding configuration,[7,8] developing new carbon and nitrogen sources,[9-15] and using co-dopants.[16-20] However, there has been relatively little discussion of the catalyst textural effects on ORR. All these carbon-based catalysts are porous in nature, which will unavoidably affect the penetration/diffusion of O_2 into the catalysts. Therefore, it is critical to understand if and how the porosity and pore size distribution affect the ORR activity. In this work, we report the synthesis of novel, metal-free porous ionic liquid (IL) derived nitrogen-doped carbons as efficient catalysts for oxygen reduction in alkaline environment. The catalysts exhibit high activities in terms of both high current densities and low overpotentials, compared to the widely used Pt/C catalyst. Our investigation shows that the pore size distribution of the catalyst is a key factor in ORR activity, and that hierarchical micro- and meso- porous structure benefits the activity.

An IL is a type of molten salts usually with organic cations and inorganic anions, and having a melting point below 100°C.[21] IL derived N-doped carbons are prepared from three functionalized ILs, based upon two different cations (ethyl or nonyl linked bis(N-(-2-cyanoethyl)-imidazole (EBi^{2+} or NBi^{2+})) and two different anions (bis(trifluoromethylsulfonyl)-imide or bis(pentafluoroethylsulfonyl)-imide (T^- or B^-)), and are totally free of metal contaminations (Fe, Ni, or Co) that have been considered as the active sites for the ORR.[22,23] The catalysts were obtained by carbonizing the IL for two hours at either 850 or 950°C under 4% H_2/Ar. The final catalysts are labeled according to the starting material and carbonization temperature (i.e. EBi-T/850). During the calcination, the nitrile groups on the cations crosslinked together, which allows the strong incorporation of N in carbon networks, while the pore size distribution was dependent upon the anion templates and the alkyl chain length.[24]

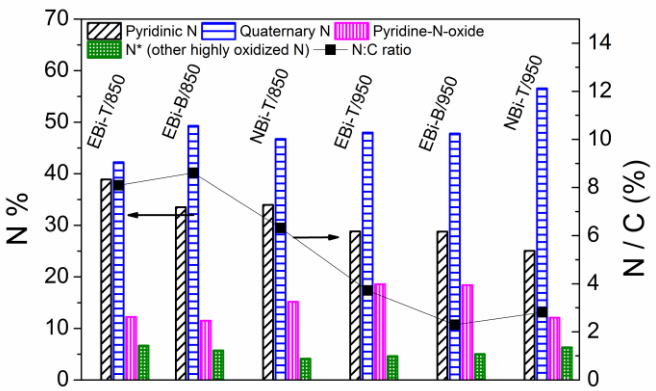

Fig.1 N composition and N/C determined by XPS on different catalysts

The chemical nature of IL-derived carbons were analysed using XPS. Besides the expected C, N and O components, the wide scans in Fig.S1, summarized in Table S1, show that S and F are detected in low concentrations in the catalysts that were carbonized at 850°C, due to incomplete decomposition of anion groups. However, S and F were not detected after the carbonization temperature increased to 950°C. No detectable transition metal species were observed by XPS. It is noted that the N/C ratio (Fig.1) also decreased when the carbonization temperature was increased from 850 to 950°C, due to the removal of less stable N containing species. Multi-component fits to the N 1s XPS spectra are presented in Fig.S2, indicating all

catalysts can be described by four different components. The obtained binding energies (eV) are assigned as pyridinic N (398.2), quaternary N (400.9 eV), and pyridine-N-oxide (402.8 eV),[7,14] while the weak peak near 405.4 eV is attributed to other highly oxidized N*.[25] The quantitative analyses (Fig.1 and Table S2) indicates that quaternary N is the most abundant N type in all the catalysts, while at the same carbonization temperature, the N compositions and N/C ratios are similar in catalysts derived from all three types of starting materials.

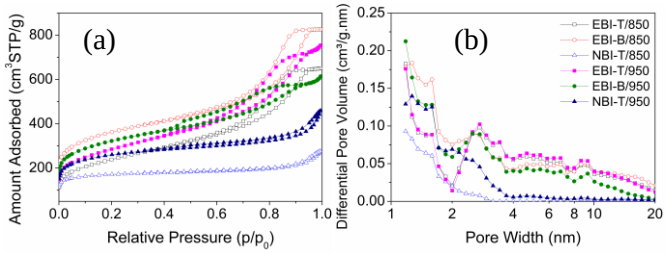

Fig.2 (a) N_2 -196°C isotherms and (b) PSDs of different catalysts.

The pore textures of IL-derived carbons were investigated by SEM (Fig.S3) and N_2 isotherms (Fig.2). The representative SEM images indicate all catalysts have a three dimensional disordered porous network. The nitrogen isotherms at -196°C (Fig.2(a)) show that all the EBi-derived carbons have type IV isotherms with H2 hysteresis loops, while NBi-T derived carbons have type I isotherms. The calculated PSDs (Fig.2(b)) for both NBi-T derived carbons exhibit mainly micropores with the maxima pore widths ~ 1.2 nm,[24] while EBi-T and -B derived carbons also exhibit a wide range of mesopore from 2 to 20 nm. Due to the combination of micro- and meso- pore structure, the EBi-derived carbons exhibit higher surface area (Table S3). For example, the surface area of EBi-B/850 is 1277 $m^2\ g^{-1}$, roughly twice that of NBi-N/850 (588 $m^2\ g^{-1}$).

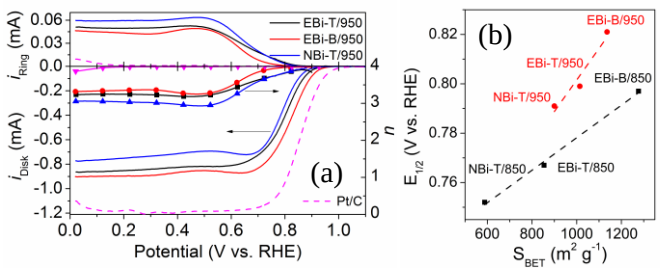

Fig.3 (a) Disk (lower part) and ring current (upper part), and number of transferred electrons, *n*, (symbol line) during the anodic scan on catalysts prepared at 950°C, 1600 rpm; (b) $E_{1/2}$–S_{BET} plot on different IL-derived carbons.

The electrocatalytic activities of IL-derived carbons were investigated and the results are summarized in Fig.3, Fig.S4 and S5. In the absence of O_2, EBi-B/950 only shows a typical double-layer capacitive CV profile in 0.1 M KOH (Fig.S4(a)), with no typical oxidation/reduction peaks. When O_2 is supplied, it is clear that a large reduction current was generated just below 1.0 V in both cathodic and anodic scans, indicating a high activity towards oxygen reduction on this catalyst. The oxygen reduction reaction on these IL-derived carbons was further studied and compared to commercial Pt/C (20 wt%) by linear scan voltammetry using rotating ring disk electrode (RRDE), and the polarization curves on the anodic scans after background correction are summarized in Fig.3(a) and Fig.S4(b). The number of transferred electron (*n*) is calculated from the ring and disc currents using Eq S1, and is observed to be greater than 3.0 on all the catalysts in the whole investigated potential range, indicating that the full reduction of O_2 to OH^- is predominant. The average value of *n* from 0 – 0.9 V varies with both IL precursors and carbonization temperature. For example, the average value is 3.05 and 3.31 for NBi-T/850 and EBi-B/850, respectively. When carbonized at 950°C, the highest value of 3.51 is obtained on EBi-B/950. Meanwhile, the half wave potentials, $E_{1/2}$, determined from the anodic scans on all catalysts also varies significantly with IL precursors and carbonization temperature. The highest value of 0.821V is observed on EBi-B/950, which is only about 35 mV below that on Pt/C (0.856 V). In a stability test, the EBi-B/950 still maintained 72% of its original activity after an 18 hour run at 0.55 V (Fig.S6). The RRDE analyses indicate that the both precursor and annealing temperature are key factors to ORR activity.

Both pyridinic[8,14,23] and quaternary N[26,27] have been considered responsible for the ORR activity. In our study, the combination of results in Fig.1 and Fig.3 shows that when using the same starting material, a higher carbonization temperature leads to a higher proportion of quaternary N, a lesser concentration of pyridinic N, and a higher ORR activity, indicating that quaternary N may serve to form active sites. In the meantime, when comparing three catalysts carbonized at the same temperature, we found the $E_{1/2}$ monotonically increases with the BET surface areas (Fig.3(b)). As the N composition varies only in a very small range at a certain carbonization temperature, these results indicate that the ORR activity is also controlled by the porous structure.

To further gain the insight in how pore texture affects ORR activity, and to understand if it is just a simple surface area enlargement issue or also related with the kinetics, the Koutechy-Levich (K-L) plots on EBi-B/950, EBi-T/950, and NBi-T/950 were analysed (Fig 4(a) and Fig S7) based upon Eq (1). However, due to the non-negligible pore effects, the intercept (i'^{-1}) obtained from extrapolation, can't be simply related to kinetic current i_k, but must consider pore limiting current i_p according to Eq (2). The pore limiting current depends upon the porosity, pore structure and distribution, and their surface chemical composition and states.

$$\frac{1}{i}=\frac{1}{i'}+\frac{1}{i_{Lev}}=\frac{1}{i'}+\frac{1}{0.62nFAC_0D_0^{\frac{2}{3}}\upsilon^{-\frac{1}{6}}\omega^{\frac{1}{2}}} \quad \text{Eq (1)}$$

$$\frac{1}{i'}=\frac{1}{i_k}+\frac{1}{i_p} \quad \text{Eq (2)}$$

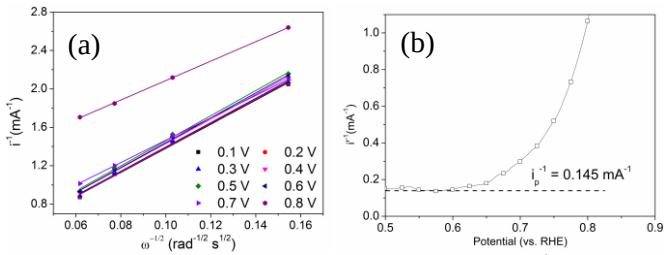

Fig.4 Representative Koutechy-Levich plot (a) and i'^{-1} plot (b) of EBi-B/950.

Since both i_k and i_p are assumed independent of the rotation frequency ω, their values cannot be distinguished independently from K-L plots. A complete understanding of i_p is complicated since it is controlled by multiple factors. However, we noticed that in the mixed kinetic-diffusion control region (0.6 ~ 0.9 V), the dramatic current increase is mainly due to the increase in kinetic component. Compared to the large increases in i_k, the changes in i_p should be insignificant. Therefore, we simplified the situation by considering i_p as a constant value that will not change with the electrode potential. Based on this assumption, the value of i_p and i_k was estimated through a typical analysis procedure presented in Fig.4(b) and Fig S8 by plotting the K-L intercepts, i'^{-1}, as a function of electrode potential. As i_k increases exponentially with the overpotential, at

high overpotentials (low electrode potentials), the contribution of i_k^{-1} becomes insignificant, while the quantity of i_p^{-1} is approaching to i'^{-1}. As a result, a plateau was reached at potentials < 0.6 V, which indicates the value of i_p^{-1}. Using this method, the pore limiting current is calculated as 5.41, 6.90, and 3.92 mA for EBi-T/950, EBi-B/950, and NBi-T/950, respectively. The large differences in the pore limiting current on different catalysts clearly show that the pore texture of the carbon-based catalyst is an important factor that cannot be neglected during the ORR activity studies. It needs to be noted that when assuming O_2 is reduced through a fully 4-e$^-$ pathway, i_{Lev} is ~ 0.52 – 1.31 mA at the rotating rate of 400 – 2500 rpm, which is of the same order as the pore limiting current. As a result, neglecting the pore limiting current will lead to large errors in determining i_k.

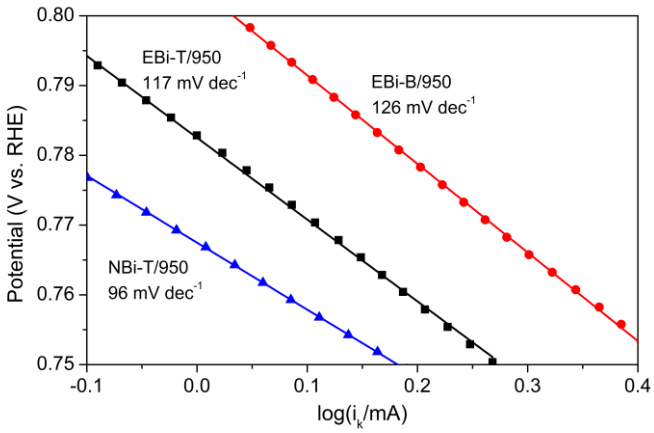

Fig.5 Tafel plots of catalysts derived at 950°C

Given the pore limiting current, the kinetic current i_k is then calculated by Eq (2). By plotting electrode potentials vs. the logarithm of i_k, the Tafel plots shown in Fig.5 were obtained. The Tafel plots are linear for all the catalysts carbonized at 950°C, indicating the mass transfer effect can be eliminated by this method. The slopes calculated from EBi-B/950 and EBi-T/950 are close to 120 mV dec^{-1}, indicating on these two catalysts the first electron transfer is the rate determining step. However, the value on NBi-T/950 is only 96 mV dec^{-1}, indicating a more complicated rate determining step that may involves both electron transfer and migration of an intermediate.[28] The sharp difference in Tafel slopes on different IL-derived carbons indicates that the pore shape and distribution also affect the ORR kinetics.

Recently, it is proposed that in alkaline electrolyte, the first step during oxygen reduction happens through an outer sphere electron transfer to form $(O_2^{\bullet-})_{aq}$, which is followed by desolvation and adsorption to form $(O_2^{\bullet-})_{ad}$. In the case of EBi-T/950 and EBi-B/950, the combination of small micropore and large mesopore allows the desolvation and adsorption steps to occur efficiently. Therefore, the overall reaction is controlled by the first electron transfer with a Tafel slope of 120 mV dec^{-1}. If the second step is much slower than the first one, the Tafel slope will be 60 mV dec^{-1}. NBi-T/950 has mainly small micropores, which limits the reaction rate of the second step. The mixed control between the first and second step leads to a Tafel slope of 96 mV dec^{-1}.

In summary, IL-derived carbons are prepared and demonstrated as a new type of highly active metal-free catalyst for oxygen reduction, via primarily a 4-e$^-$ pathway and with an overpotential only slightly larger than Pt/C. The results are the first demonstration that the pore size distribution is of significance in ORR activity in carbon-based catalysts. Pores limit diffusion and also the rates of elementary steps in ORR.

This work was supported as part of the FIRST Center, an Energy Frontier Research Center funded by the U.S. Department of Energy, Office of Science, Office of Basic Energy Sciences. A portion of this work (BET, XPS) was supported by the U.S. Department of Energy, Basic Energy Sciences, Materials Sciences and Engineering Division.

Notes and references

[a] Chemical Sciences Division, Oak Ridge National Laboratory, Oak Ridge, TN 37831

[b] Materials Sciences and Technology Division, Oak Ridge National Laboratory, Oak Ridge, TN 37831.

Electronic Supplementary Information (ESI) available: [details of any supplementary information available should be included here]. See DOI: 10.1039/c000000x/

1. K. Gong, F. Du, Z. Xia, M. Durstock and L. Dai, *Science*, 2009, **323**, 760-764.
2. L. Qu, Y. Liu, J.-B. Baek and L. Dai, *Acs Nano*, 2010, **4**, 1321-1326.
3. E. Biddinger, D. Deak and U. Ozkan, *Top. Catal.*, 2009, **52**, 1566-1574.
4. Y. Shao, S. Zhang, M. H. Engelhard, G. Li, G. Shao, Y. Wang, J. Liu, I. A. Aksay and Y. Lin, *J. Mater. Chem.*, 2010, **20**, 7491-7496.
5. W. Yang, T.P. Fellinger and M. Antonietti, *J. Am. Chem. Soc.*, 2010, **133**, 206-209.
6. T. C. Nagaiah, A. Bordoloi, M. D. Sánchez , M. Muhler and W. Schuhmann, *ChemSusChem*, 2012, **5**, 637-641.
7. L. Lai, J. R. Potts, D. Zhan, L. Wang, C. K. Poh, C. Tang, H. Gong, Z. Shen, J. Lin and R. S. Ruoff, *Energy Environ. Sci.*, 2012, **5**, 7936-7942.
8. S. Yasuda, L. Yu, J. Kim and K. Murakoshi, *Chem. Comm.*, 2013, **49**, 9627-9629.
9. H. Zhu, J. Yin, X. Wang, H. Wang and X. Yang, *Adv. Funct. Mater.*, 2013, **23**, 1305-1312.
10. H. Zhong, H. Zhang, S. Liu, C. Deng and M. Wang, *ChemSusChem*, 2013, **6**, 807-812.
11. S.A. Wohlgemuth, T.P. Fellinger, P. Jaker and M. Antonietti, *J. Mater. Chem. A*, 2013, **1**, 4002-4009.
12. Z. Lin, G. H. Waller, Y. Liu, M. Liu and C. P. Wong, *Carbon*, 2013, **53**, 130-136.
13. Z. Lin, G. H. Waller, Y. Liu, M. Liu and C. P. Wong, *Nano Energy*, 2013, **2**, 241-248.
14. X. Q. Wang, J. S. Lee, Q. Zhu, J. Liu, Y. Wang and S. Dai, *Chem. Mater.*, 2010, **22**, 2178-2180.
15. D. Geng, Y. Chen, Y. Chen, Y. Li, R. Li, X. Sun, S. Ye and S. Knights, *Energy Environ. Sci.*, 2011, **4**, 760-764.
16. J. Xu, G. Dong, C. Jin, M. Huang and L. Guan, *ChemSusChem*, 2013, **6**, 493-499.
17. X. Sun, Y. Zhang, P. Song, J. Pan, L. Zhuang, W. Xu and W. Xing, *ACS Catalysis*, 2013, 1726-1729.
18. S. Inamdar, H.-S. Choi, P. Wang, M. Y. Song and J.-S. Yu, *Electrochem. Commun.*, 2013, **30**, 9-12.
19. C. H. Choi, M. W. Chung, H. C. Kwon, S. H. Park and S. I. Woo, *J. Mater. Chem. A*, 2013, **1**, 3694-3699.
20. Z. W. Liu, F. Peng, H. J. Wang, H. Yu, W. X. Zheng and J. Yang, *Angew. Chem. Int. Ed.*, 2011, **50**, 3257-3261.
21. Z. Ma, J. Yu and S. Dai, *Adv. Mater.*, 2010, **22**, 261-285.

22. M. Lefèvre, E. Proietti, F. Jaouen and J. P. Dodelet, *Science*, 2009, **324**, 71-74.
23. P. H. Matter, L. Zhang and U. S. Ozkan, *J. Catal.*, 2006, **239**, 83-96.
24. P. F. Fulvio, P. C. Hillesheim, Y. Oyola, S. M. Mahurin, G. M. Veith and S. Dai, *Chem. Commun.*, 2013, **49**, 7289-7291.
25. J. R. Pels, F. Kapteijn, J. A. Moulijn, Q. Zhu and K. M. Thomas, *Carbon*, 1995, **33**, 1641-1653.
26. R. Liu, D. Wu, X. Feng and K. Müllen, *Angew. Chem. Int. Ed.*, 2010, **49**, 2565-2569.
27. H. Kim, K. Lee, S. I. Woo and Y. Jung, *Phys. Chem. Chem. Phys.*, 2011, **13**, 17505-17510.
28. G. Wu, K. L. More, C. M. Johnston and P. Zelenay, *Science*, 2011, **332**, 443-447.

Table of contents:

Pore size distribution in ionic liquid derived N-doped carbons affects both activity and kinetics in the oxygen reduction reaction.